ORIGINAL ARTICLE

Phenolic compounds of *Solanum xanthocarpum* play an important role in anti-inflammatory effects

Zhen-Peng Xu [1], **Yan Liu** [1], **Si-Yi Wang, Zi-Wei Li, Dong-Xu Lu, Peng Jiang, Juan Pan, Wei Guan, Hai-Xue Kuang** [*], **Bing-You Yang** [*]

Key Laboratory of Basic and Application Research of Beiyao (Heilongjiang University of Chinese Medicine), Ministry of Education, Heilongjiang University of Chinese Medicine, Harbin 150040, China

Abstract *Solanum xanthocarpum* is used for the treatment of rheumatic arthritis, toothache, sore throats, carbuncle, furuncle, and other inflammatory diseases in traditional Chinese medicine and Ayurvedic medical system, with the phenolic compounds being one of its principal components. In this study, 51 phenolic compounds including seven new compounds **1**, **2**, **9**, **13**, **17**, **22**, and **40** were isolated from the fruits of *Solanum xanthocarpum*. 40 known compounds **3–8**, **10–12**, **14–16**, **18–21**, **23–25**, **28–32**, **35–39**, **41–51** were firstly isolated from *Solanum xanthocarpum*. Their structures were determined by comprehensive spectroscopic analyses, X-ray crystallography, NMR calculations, chemical methods, and comparisons of spectroscopic data. The results of anti-inflammatory assays indicated that most isolated compounds (**3–7**, **11–30**, **32–37**, **39**, **40**, **42**, **43**, **45**, and **48–51**) possessed significant inhibitory activities of the NO release of LPS-induced RAW 264.7 cells, with IC_{50} values ranging from 10.46 to 47.59 μM. Further analysis by molecular docking implied that most bioactive compounds could interact with the amino acid residues of iNOS proteins, supporting the anti-inflammatory activity of the compounds. Especially, compounds **17–20**, **26–27**, **32**, and **34** showed strong affinities with iNOS proteins. The bioinformatic analysis further revealed the potential anti-inflammatory targets of the phenolic compounds isolated from the fruits of *Solanum xanthocarpum*.

© 2022 The Author(s). Published by Elsevier B.V. on behalf of King Saud University. This is an open access article under the CC BY-NC-ND license (http://creativecommons.org/licenses/by-nc-nd/4.0/).

1. Introduction

* Corresponding authors.
 E-mail addresses: hxkuang@yahoo.com (H.-X. Kuang), yby-water@163.com (B.-Y. Yang).
 [1] These authors contributed equally to this work.
Peer review under responsibility of King Saud University.

Solanum xanthocarpum is widely distributed in southern areas of China, India, Arabia, Sri Lanka, Malaysia, Vietnam, Thailand, and other tropical areas. *Solanum xanthocarpum* is used for the treatment of rheumatic arthritis, toothache, sore throats, carbuncle, furuncle, and other inflammatory diseases in traditional Chinese medicine and Ayurvedic medical system (Kar et al., 2006; More et al., 2013; Parmar et al., 2017; Periyannan et al., 2016; Shivnath et al., 2021). In a previous study, whole parts of *Solanum xanthocarpum* have shown

anti-inflammatory activity against carrageenan and histamine-induced paw edema (More et al., 2013). In addition, *Solanum xanthocarpum* fruits extract has ameliorated osteoarthritis development in collagenase-induced osteoarthritic rats (Shivnath et al., 2021). The phenolic compounds are one of the principal components of *Solanum xanthocarpum* fruits. The total phenolic content of *Solanum xanthocarpum* fruits was found to be 462 mg per g dry weight of extract (Shivnath et al., 2021). Phenolic compounds could inhibit either the production or the action of pro-inflammatory mediators, resulting in anti-inflammatory capacity. And phenolic compounds have been shown to play important anti-inflammatory roles in some plants. (Ambriz-Pérez et al., 2016; Barakat et al., 2020). Hence, this research investigated the isolation, structural characterization, and anti-inflammatory effects assessments of the phenolic compounds from the *Solanum xanthocarpum* fruits.

2. Materials and methods

2.1. General experimental procedures

HRESIMS spectra were performed on an UHPLC-Orbitrap-MS instrument or an AB SCIEX Triple TOF 5600 instrument. NMR spectra were obtained on a Bruker DPX 600 instrument (600 MHz for ^{1}H NMR and 150 MHz for ^{13}C NMR) or a Bruker DPX 400 instrument (400 MHz for ^{1}H NMR and 100 MHz for ^{13}C NMR) with TMS as an internal standard. Optical rotations were measured by a JASCO P-2000 digital polarimeter. CD spectra were recorded on a Bio-Logic Science MOS-450 spectropolarimeter. IR spectra were recorded on a Thermo Scientific Nicolet FTIR-8400S spectrometer with KBr panels. X-ray data were obtained from a Bruker D8 Venture instrument. Preparative HPLC was performed on LC-20AR HPLC equipped with RID-20A detector (Shimadzu Corporation) coupled with a Waters SunFire C18 prep column (10 × 250 mm, 5 μm). Column chromatography was carried out using silica gel (200–300 mesh, Qingdao Marine Chemical Ltd., China), MCI gel (CHP 20, Mitsubishi Chemical Industries Ltd., Japan), and octadecyl silica gel (YMC Company Ltd., Japan). Fractions were monitored by TLC (silica gel GF$_{254}$ plates) and HPLC performed on Waters e2695–2424–2998 system. GC–MS analysis was performed on an Agilent Technologies (7890A) system with a DB-5 capillary column.

2.2. Plant material

The fruits of *Solanum xanthocarpum* were collected from Guilin of Guangxi Province and identified by Prof. Rui-Feng Fan. A voucher specimen (No. 20160327) was deposited in the laboratory at the School of Pharmacy, Heilongjiang University of Chinese Medicine.

2.3. Extraction and isolation

The air-dried fruits of *Solanum xanthocarpum* (9 kg) were crushed and extracted with 70% ethanol (54 L × 3, each for 2 h) under reflux. The extract was filtered and then concentrated in vacuo to get the crude extract (2473.6 g). Then the crude extract was suspended in water and subsequently partitioned with petroleum ether, EtOAc, and *n*-BuOH to obtain 34.0, 150.1, 393.8, and 1605.0 g of extracts, respectively.

The crude EtOAc fraction (100.0 g) was separated by open silica gel column chromatography, ODS-MPLC, semipreparative HPLC, and preparative HPLC to yield **21–28, 32, 33, 37,** and **40.** The crude *n*-BuOH fraction (280.0 g) was separated by open silica gel column chromatography, ODS-MPLC, semipreparative HPLC, and preparative HPLC to yield **1, 2, 4–20, 29, 31, 34–36, 38, 39, 41–44,** and **46–51.** The crude water fraction (1000.0 g) was dissolved in water (2.0 L) and 95% alcohol (8.0 L) was added to it with full stirring. Then the supernatant was filtered after that the mixture was refrigerated at 4 °C for 12 h. The supernatant was concentrated in vacuo to get the crude extract (86.6 g). The crude extract was separated by AB-8 macroporous resin column chromatography, MCI column chromatography, and semipreparative HPLC to yield **3, 30,** and **45.** For the details of separation procedures for **1–51,** see the "Extraction and isolation" section in the Supplementary material.

2.3.1. Chlorogenic acid ethyl ester-4′-O-β-D-glucopyranoside (1)

Colorless crystals (MeOH); [α]17 D −48.0 (c 0.10, MeOH); UV λ$_{max}$ (MeOH): 292 nm; IR ν$_{max}$ 3409, 2927, 1698, 1635, 1508, 1449, 1394, 1269, 1128, 1074, and 617 cm^{-1}; HRESIMS *m/z* 543.1720 [M−H]$^-$ (calcd. 543.1719); ^{1}H NMR (methanol d$_4$, 400 MHz) and ^{13}C NMR (methanol d$_4$, 100 MHz) spectra data see Table 1.

2.3.2. Chlorogenic acid methyl ester-4′-O-β-D-glucopyranoside (2)

White amorphous powder; [α]17 D −62.0 (c 0.10, MeOH); UV λ$_{max}$ (MeOH): 294 nm; IR ν$_{max}$ 3391, 2922, 1732, 1634, 1509, 1453, 1394, 1269, 1128, 1074, and 612 cm^{-1}; HRESIMS *m/z* 529.1564 [M−H]$^-$ (calcd. 529.1563); ^{1}H NMR (methanol d$_4$, 400 MHz) and ^{13}C NMR (methanol d$_4$, 100 MHz) spectra data see Table 1.

2.3.3. (7R,8S)-threo-glehlinoside C (9)

White amorphous powder; [α]17 D −56.0 (c 0.10, MeOH); UV λ$_{max}$ (MeOH): 232, 322 nm; CD λ$_{max}$ (MeOH, c 0.91 mM) nm (Δε): 240 (+2.61), 302 (−0.43); IR ν$_{max}$ 3559, 3440, 3379, 3235, 1637, 1616, 1267, and 626 cm^{-1}; HRESIMS *m/z* 551.1770 [M−H]$^-$ (calcd. 551.1770); ^{1}H NMR (methanol d$_4$, 400 MHz) and ^{13}C NMR (methanol d$_4$, 100 MHz) spectra data see Table 2.

2.3.4. 2Z-(7S,8R)-aegineoside (13)

White amorphous powder; [α]18 D −6.0 (c 0.10, MeOH); UV λ$_{max}$ (MeOH): 207, 282 nm; CD λ$_{max}$ (MeOH, c 0.94 mM) nm (Δε): 238 (+2.20), 324 (+0.35); IR ν$_{max}$ 2930, 1701, 1599, 1514, 1267, 1220, 1073, and 548 cm^{-1}; HRESIMS *m/z* 533.1664 [M−H]$^-$ (calcd. 533.1664); ^{1}H NMR (methanol d$_4$, 400 MHz) and ^{13}C NMR (methanol d$_4$, 100 MHz) spectra data see Table 2.

2.3.5. (7R,8R)-3,5-dimethoxy-8′-carboxy-7′-en-3′,8-epoxy-7,4′-oxyneolignan-4,9-diol (17)

White amorphous powder; [α]17 D −22.0 (c 0.10, MeOH); UV λ$_{max}$ (MeOH): 213, 288 nm; IR ν$_{max}$ 2027, 1637, 1616, 1119, and 622 cm^{-1}; HRESIMS *m/z* 389.1240 [M+H]$^+$ (calcd.

Table 1 ^{1}H NMR and ^{13}C NMR data (δ in ppm, recorded in methanol d_4) of **1** and **2**.

No.	1		2	
	δ_C	δ_H	δ_C	δ_H
1	75.8		75.9	
2	37.9	2.01, dd (13.2, 6.9)	38.0	2.01, dd (13.8,6.9)
		2.21, o		2.20, o
3	70.5	4.14, m	70.4	4.11, m
4	72.7	3.73, o	72.7	3.72, o
5	72.3	5.28, m	72.3	5.28, m
6	38.0	2.13, o	38.0	2.14, o
		2.18, o		2.18, o
7	175.0		175.4	
8	62.5	4.19, o	53.0	3.69, s
9	14.3	1.24, t (7.1)		
1'	131.0		131.0	
2'	115.9	7.10, d (2.0)	115.9	7.06, d (2.0)
3'	148.6		148.6	
4'	149.0		149.0	
5'	118.1	7.20, d (8.4)	118.1	7.20, d (8.4)
6'	122.2	7.04, dd (8.4, 2.0)	122.2	7.04, dd (8.4, 2.0)
7'	146.3	7.56, d (16.0)	146.4	7.55, d (16.0)
8'	117.3	6.32, d (16.0)	117.3	6.32, d (16.0)
9'	167.9		167.9	
1''	103.5	4.85, o	103.5	4.84, o
2''	74.8	3.51, dd (9.1, 7.5)	74.8	3.50, o
3''	77.5	3.49, o	77.6	3.48, o
4''	71.3	3.42, o	71.3	3.40, o
5''	78.4	3.44, o	78.4	3.44, o
6''	62.4	3.72, dd (12.1,5.2)3.90, dd (12.1,1.9)	62.4	3.70, o3.90, dd (12.0,1.7)

"o" means overlapped with other signals.

389.1231); ^{1}H NMR (methanol d_4, 400 MHz) and ^{13}C NMR (methanol d_4, 100 MHz) spectra data see Table 3.

2.3.6. 3-(4-hydroxy)-N-[2-(3-methoxyphenyl-4-hydroxyphenyl)-2- hydroxy]acrylamide (22)

White amorphous powder; [α]17 D −4.0 (c 0.10, MeOH); IR v_{max} 1638, 1617, 1515, and 622 cm^{-1}; HRESIMS m/z 328.1183 [M−H]$^-$ (calcd. 328.1190); ^{1}H NMR (methanol d_4, 600 MHz) and ^{13}C NMR (methanol d_4, 150 MHz) spectra data see Table 3.

2.3.7. p-hydroxyphenylacetonitrile-O-(6'-O-acetyl)-β-D-glucopyranoside (40)

White amorphous powder; [α]20 D + 30.0 (c 0.10, MeOH); UV λ_{max} (MeOH): 224, 291 nm; IR v_{max} 2027, 1639, 1617, 1235, 1077, and 626 cm^{-1}; HRESIMS m/z 355.1493 [M +NH$_4$]$^+$ (calcd. 355.1500); ^{1}H NMR (methanol d_4, 600 MHz) and ^{13}C NMR (methanol d_4, 150 MHz) spectra data see Table 3.

2.4. X-ray crystallographic analysis

The crystals of **1** were recrystallized from methanol. X-ray analyses of **1** were carried out on a Bruker D8 Venture diffractometer with Cu Kα radiation. The crystallographic data for compounds **1** (deposition No. CCDC 2133149) has been deposited at the Cambridge Crystallographic Data Center.

chlorogenic acid ethyl ester-4'-O-β-D-glucopyranoside (**1**). 2 ($C_{24}H_{32}O_{14}$), 2(H_2O), M = 1125.02, T = 193 K, V = 1452.84 (14), D_{calcd} = 1.286 g/cm^3, Z = 1, monoclinic, p1211, a = 13.5031(9) Å, b = 6.1589(3) Å, c = 17.9871(9) Å, α = γ = 90°, β = 103.778(4)°, F(000) = 596.0, 2.529° ≤ θ ≤ 81.283°, −16 ≤ h ≤ 16, −7 ≤ k ≤ 7, −20 ≤ l ≤ 22, Flack parameter: 0.19(13).

2.5. NMR calculations

The theoretical calculations of **22** were performed by Gaussian 09. Conformation search was performed using the program Conflex 7 Rev. C. NMR calculations of **22** were calculated with the GIAO method at mPW1PW91/6-31G*//B3LYP/6-31G* (in the gas phase) and mPW1PW91/6-31G**// B3LYP/6-31G* levels (in methanol with PCM model). The shielding constants (^{13}C and ^{1}H) obtained were performed statistical analyses with experimental data by using DP4$^+$ probability (Grimblat et al., 2015).

2.6. Acid hydrolysis and GC analysis

The compounds (**1**, **2**, **9**, **13**, and **40**) (1.0 mg each) were individually hydrolyzed and treated by the same method as described in the previous paper from this laboratory (Yin et al., 2019). The presence of D-glucose of compounds **1**, **2**, **9**, **13**, and **40** was finally confirmed by comparing the retention

Table 2　^{1}H NMR and ^{13}C NMR data (δ in ppm, recorded in methanol d_4) of **9, 10,** and **13**.

No.	9		10		13	
	δ_C	δ_H	δ_C	δ_H	δ_C	δ_H
1	137.3		137.5		137.9	
2	112.5	7.12, d (1.2)	112.8	7.11, d (1.8)	111.2	7.02, d (1.8)
3	150.5		150.4		151.0	
4	147.4		147.4		147.7	
5	117.5	7.11, d (8.4)	117.5	7.09, d (8.4)	118.0	7.14, d (8.4)
6	120.6	6.97, dd (8.4,1.2)	121.1	6.96, dd (8.4,1.8)	119.4	6.93, dd (8.4,1.8)
7	73.5	4.94, d (4.8)	73.8	4.87, o	89.2	5.63, d (5.8)
8	85.9	4.47, m	85.3	4.49, m	55.2	3.48, o
9	61.9	3.52, dd (12.0,5.6)	62.2	3.84, o	64.9	3.78, o
		3.80, o				3.84, o
1′	129.8		129.7		130.3	
2′	112.3	7.20, d (1.6)	112.3	7.15, d (1.9)	116.2	7.54, br. s
3′	151.7		151.8		144.9	
4′	151.6		151.5		150.6	
5′	117.4	7.03, d (8.4)	117.4	6.97, o	129.4	
6′	123.5	7.09, dd (8.4,1.6)	123.4	7.06, o	121.4	7.20, br. s
7′	146.1	7.57, d (15.6)	146.3	7.57, d (15.9)	143.5	6.83, d (12.8)
8′	117.7	6.36, d (15.6)	117.4	6.34, d (15.9)	118.5	5.82, d (12.8)
9′	171.0		170.8		170.6	
3-OCH$_3$	56.6	3.82, s	56.6	3.80, s	56.7	3.83, s
3′-OCH$_3$	56.7	3.88, s	56.7	3.81, s	56.7	3.87, s
1″	102.8	4.86, d (7.2)	102.9	4.83, d (7.4)	102.7	4.87, o
2″	74.9	3.48, m	74.9	3.47, o	74.9	3.48, o
3″	77.8	3.47, m	77.8	3.46, o	77.8	3.47, o
4″	71.3	3.39, o	71.3	3.39, o	71.3	3.39, o
5″	78.2	3.39, m	78.2	3.39, m	78.2	3.39, o
6″	62.5	3.68, dd (12.0,3.6)	62.5	3.68, dd (12.2,2.6)	62.5	3.85, o3.68, dd
		3.86, o		3.87, o		(12.2,4.4)

"o" means overlapped with other signals.

time with the authentic sample analyzed by Agilent 7890A GC–MS system using a DM-5 column (30 m × 0.25 mm, 0.25 μm).

2.7. Anti-inflammatory assays

The RAW 264.7 cells were cultured in the DMEM medium with 10% FBS in 96-well plates (5×10^4/well) for 24 h. Then, the RAW264.7 cells were divided into four groups containing the control group, the model group (1 μg/mL LPS), the positive control group (1 μg/mL LPS and indomethacin at final concentrations of 1.25, 2.5, 5, 10, 20 μM/mL), and the sample group (1 μg/mL LPS and the test compounds at final concentrations of 5, 10, 20, 30, 50 μM/mL) for 24 h. The NO concentration in the culture medium was measured by the Griess reagent at 540 nm (Fu et al., 2021).

2.8. Molecular docking studies

Molecular docking simulations were performed by the software Autodock 4.2.6 using the hybrid Lamarckian Genetic Algorithm. The three-dimensional crystal structure of iNOS (PDB ID: 3E6T) was obtained from the RCSB Protein Data Bank (https://www.rcsb.org/) (Zhang et al., 2020). The three-dimensional structures ("pdb" format) of ligands were constructed and the energy was minimized by Chem3D Pro 14.0. The proteins and ligands were processed by AutoDock-

Tools 1.5.6 and converted to "pdbqt" format. The search was extended over the whole receptor protein used as blind docking. Pymol 2.6.0 was applied to visualize the interactions between ligands and receptors.

2.9. Bioinformatic analysis

The database of UniProt (https://www.uniprot.org/) was used to construct inflammation-related target libraries by performing automated searches using keywords including "inflammation" and "inflammatory". The molecular targets for the "Homo sapiens" species of all isolated compounds were predicted through SwissTargetPrediction (https://www.swisstargetprediction.ch/) web tool. The compound targets and inflammation-related targets were set as the background lists to get the overlapping targets using Venn diagrams (https://bioinformatics.psb.ugent.be/webtools/Venn/) web tool. Cytoscape3.7.2 software was used to import the data to construct and visualize the compound-target network.

3. Results and discussion

3.1. Isolation and identification of compounds

51 phenolic compounds (Fig. 1) including seven new compounds (**1**, **2**, **9**, **13**, **17**, **22**, and **40**) and 44 known compounds were isolated from *Solanum xanthocarpum* fruits. These struc-

Table 3 ^{1}H NMR and ^{13}C NMR data (δ in ppm, recorded in methanol d_4) of **17**, **22**, and **40**.

No.	17 δ_C	17 δ_H	22 δ_C	22 δ_H	40 δ_C	40 δ_H
1	128.3		127.9		126.2	
2	106.0	6.74, br. s	132.4	7.39, d (8.6)	130.2	7.28, d (8.6)
3	149.5		116.0	6.72, d (8.6)	118.4	7.08, d (8.6)
4	137.4		159.3		158.6	
5	149.5		116.0	6.72, d (8.6)	118.4	7.08, d (8.6)
6	106.0	6.74, br. s	132.4	7.39, d (8.6)	130.2	7.28, d (8.6)
7	78.3	4.94, d (8.1)	138.6	6.62, d (12.7)	22.7	3.83, s
8	79.9	4.09, m	121.1	5.82, d (12.7)	119.8	
9	62.0	3.49, dd (12.4,4.3)3.72, dd (12.4,2.4)	170.5			
1′	129.7		135.4		102.1	4.89, d (7.4)
2′	117.4	7.23, d (1.8)	110.8	6.97, d (1.6)	74.8	3.45, m
3′	145.2		148.9		77.8	3.45, m
4′	147.4		147.1		71.6	3.36, m
5′	118.5	6.94, d (8.4)	116.0	6.76, d (8.0)	75.3	3.64, m
6′	123.0	7.11, dd (8.4,1.8)	120.0	6.80, dd (8.0,1.6)	64.7	4.39, d (11.9,2.1)4.23, d (11.9,6.5)
7′	145.6	7.56, d (15.9)	73.5	4.69, dd (7.7,5.1)	172.7	
8′	118.1	6.34, d (15.9)	48.0	3.49, dd (13.6,5.1)3.40, dd (13.6,7.7)	20.7	2.04, s
9′	171.6					
3-OCH$_3$	56.9	3.86, s				
5-OCH$_3$	56.9	3.86, s				
3′-OCH$_3$			56.3	3.84, s		

"o" means overlapped with other signals.

tures of the new compounds were identified by NMR and HRESIMS, and their configurations were determined by CD spectra or X-ray diffraction data.

By comparison of their experimental and reported NMR data, the known compounds were identified as 5-O-(4′-O-caffeoyl glycosyl)-quinic acid (**3**) (Crupi et al., 2018), chlorogenic acid ethyl ester (**4**) (Li et al., 2017), chlorogenic acid methyl ester (**5**) (Zhang et al., 2013b), chlorogenic acid (**6**) (Lee et al., 2010), neochlorogenic acid methyl ester (**7**) (Zhu et al., 2005), 1β,3β,4β-trihydroxy-5α-[[3-[4-[1β-(6-O-(E)-sinapoyl-β-D- glucopyranosyl)oxy]-3-hydroxyphenyl]-(E)-1-oxo-2-propenyl]oxy] cyclohexanecarboxylic acid (**8**) (Ma et al., 2010), (7S,8S)-*erythro*-glehlinoside C (**10**) (Yuan et al., 2002), (7S,8S)-*erythro*-guaiacylglycerol-β-ferulic acid ether (**11**) (Liu et al., 2018), (7R,8S)-*threo*-guaiacylglycerol-β-ferulic acid ether (**12**) (Liu et al., 2018), dehydrodiconiferyl alcohol-4-O-β-D-glucopyranoside (**14**) (Iclal et al., 2003), dehydrodiconiferyl alcohol 9′-methyl ether-4-O-β-D-glucoside (**15**) (Xiao et al., 2017), (7S,8R)-dehydrodiconiferyl alcohol 4,9′-di-O-β-D-glucopyranoside (**16**) (Wang et al., 2017), (7R,8R)-3-methoxy-8′-carboxy-7′-en-3′,8-epoxy-7,4′-oxyneo lignan- 4,9-diol (**18**) (Zhou et al., 2015), pinonesinol (**19**) (Zhou et al., 2004), epipinoresinol (**20**) (Yang et al., 2015), (−)-syringaresinol-4-O-β-D-glucopyranoside (**21**) (Ding et al., 2011), N-cis-feruloyloctopamine (**23**) (Yin et al., 2018), N-cis-p-coumaroyloctopamine (**24**) (Yang et al., 2018), melonge-namide H (**25**) (Zhao et al., 2021), N-trans-p-coumaroyltyramine (**26**) (Zhao et al., 2021), trans-N-coumaroyltyramine (**27**) (Al-Taweel et al., 2012), N-trans-feruloyloctopamine (**28**) (Li et al., 2009), sophoraflavonoloside (**29**) (Abdallah et al., 2014), isorhamnetin 3,7-O-di-β-D-glucopyranoside (**30**) (Sasaki and Takahashi, 2002), solanofla-

vone (**31**) (Shen et al., 2005), (+)-taxifolin (**32**) (Shen et al., 2010), caffeic acid (**33**) (Chen et al., 2008), caffeic acid methyl ester (**34**) (Zhao et al., 2002), caffeic acid 4-O-β-D-glucopyranoside (**35**) (Liang et al., 2010), 4-allyl-2,6-dimethoxyphenol glucoside (**36**) (Li et al., 2004), citrusin C (**37**) (Takeda et al., 1998), syringin (**38**) (Zhao et al., 2006), 3-(4-hydroxy-3-methoxy phenyl)propan-1,2-diol (**39**) (Uyang et al., 2007), hydranitriloside B2 (**41**) (Wang et al., 2011), 2-(4-hydroxyphenyl)-ethanol (**42**) (Lou et al., 2001), salidroside (**43**) (Saimaru and Orihara, 2010), 2-(4-hydroxyphenyl) ethanol-O-β-D-glucopyranosyl-(1 → 2)-O-β-D-glucopyranoside (**44**) (Kuang et al., 2018), (methoxycarbony-lmethyl)phenyl-4-O-β-D-glucopyranoside (**45**) (Liang et al., 2013), 2-(sophorosyl)-1- (4-hydroxyphenyl) ethanone (**46**) (Jin et al., 2014), foliachinenosides A2 (**47**) (Nakamura et al., 2008), 4-methoxybenzyl-β-D-glucopyranoside (**48**) (Zhang et al., 2013a), gaultherin (**49**) (He et al., 2017), 4-hydroxyphenyl β-D-glucopyranosyl-(1 → 2)-β-D-glucopyrano-side (**50**) (Ono et al., 2008), p-hydroxyphenyl-O-β-D-primeveroside (**51**) (Ralf et al., 1993). Among them, 40 compounds **3–8, 10–12, 14–16, 18–21, 23–25, 28–32, 35–39, 41–51** were isolated from *Solanum xanthocarpum* for the first time.

Compound **1**, colorless crystals, gave the molecular formula of $C_{24}H_{32}O_{14}$ based on its HRESIMS spectrum (m/z 543.1720 [M−H]$^-$, calcd. 543.1719). The ^{1}H NMR data (Table 1) showed the presence of a set of ABX systems at δ_H 7.20 (H-5′), 7.10 (H-2′), and 7.04 (H-6′), and two olefinic protons at δ_H 7.56 (H-7′) and 6.32 (H-8′). Two methylene signals at δ_H 2.21 (H-2a), 2.01 (H-2b), 2.18 (H-6a), and 2.13 (H-6b), and a methyl signal at δ_H 1.24 (H-9) were also observed. In addition, 12 proton signals at δ_H 3.42–5.28 implied the presence of a
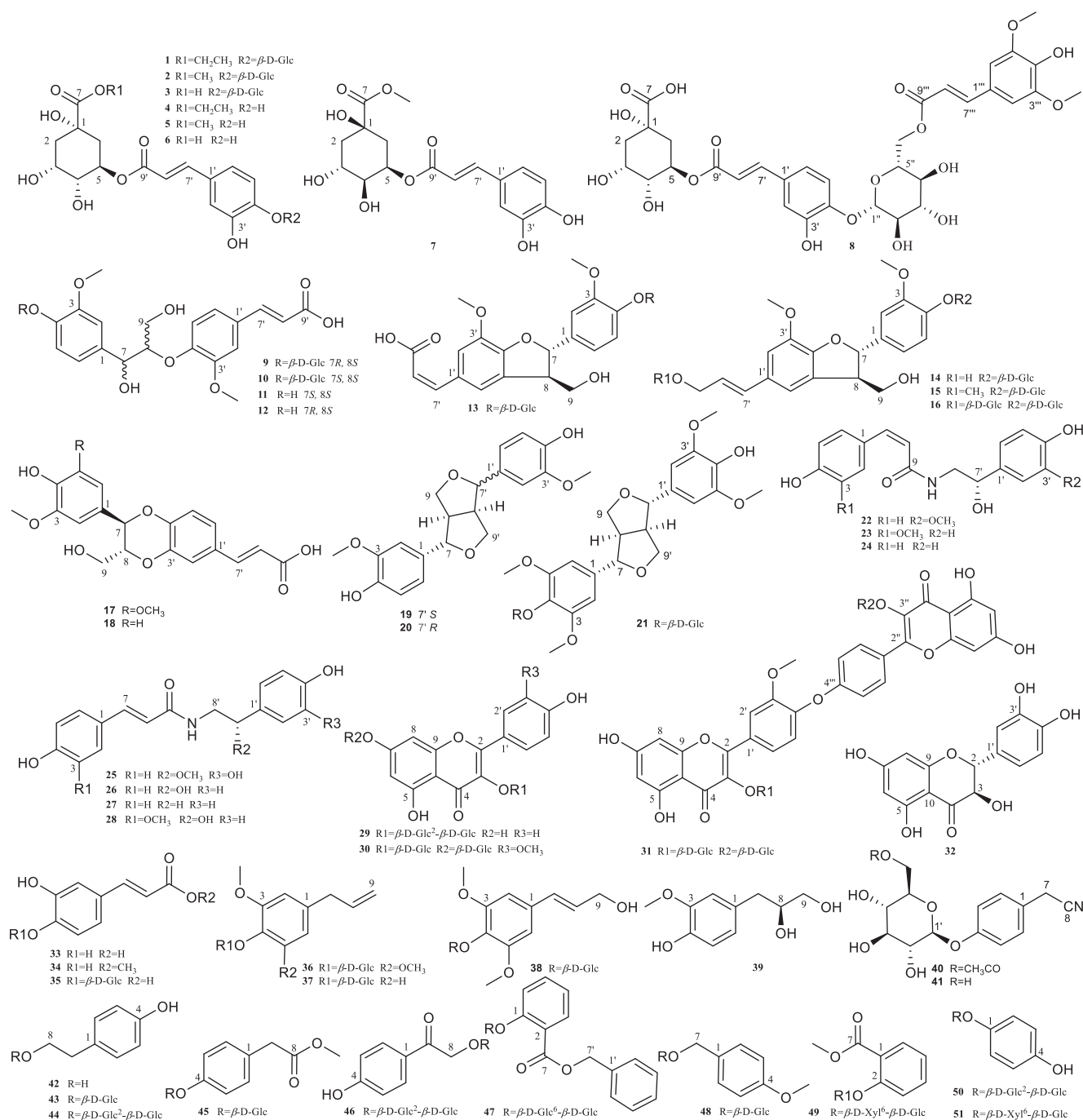
Fig. 1 Chemical structures of compounds **1–51**.

β-glucose and 3 oxo-methine signals, an oxo-methylene signals of the aglycone. Its ^{13}C NMR spectrum (Table 1) indicated the presence of 24 carbons including a group of β-glucose at δ_C 103.5, 78.4, 77.5, 74.8, 71.3, 62.4, and an alcohol group at δ_C 62.5, 14.3. The remaining 16 carbons were consistent with those of chlorogenic acid (**6**) (Lee et al., 2010). The HMBC correlations from δ_H 4.85 (H-1″) to 149.0 (C-4′), δ_H 4.19 (H-8) to 175.0 (C-7) established the connection of the β-glucose and the alcohol group to the chlorogenic acid unit. Assignments of all groups of **1** were achieved by HSQC, ^{1}H–^{1}H COSY, and HMBC data (Fig. 2). A thin crystal of **1** was

obtained from methanol, and X-ray diffraction analysis was performed with Cu Kα (Fig. 3). Hence, the absolute configurations of **1** were unambiguously determined to be 1S, 3R, 4R, and 5R consistent with them of chlorogenic acid. Therefore, the structure of **1** was identified as chlorogenic acid ethyl ester-4′-O-β-D-glucopyranoside. Compound **1** was confirmed to be an artificial product by analysis of the 70% methanol extract of *Solanum xanthocarpum* fruits by UHPLC-MS (Figs. S154–S155).

Compound **2** was purified as a white amorphous powder with the molecular formula of $C_{23}H_{30}O_{14}$, deduced from the
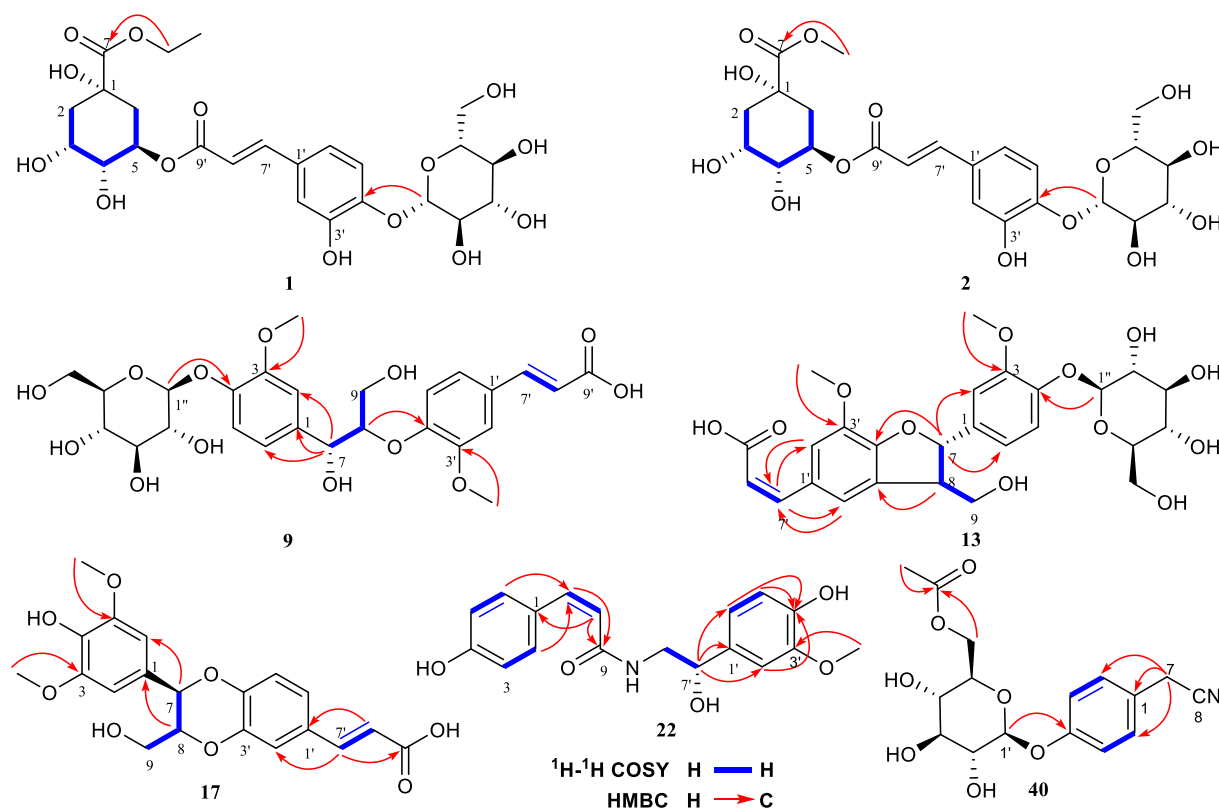
Fig. 2 ¹H–¹H COSY and key HMBC correlations of compounds **1**, 2, **9**, **13**, **17**, **22,** and **40**.

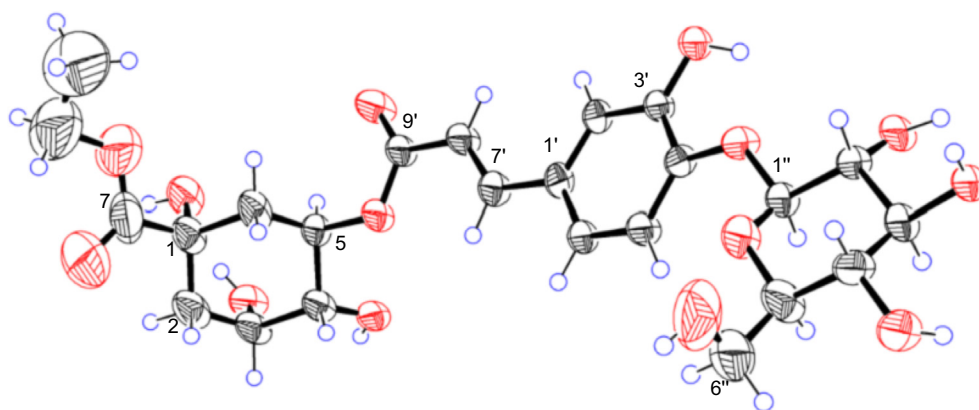**Fig. 3** Single-crystal X-ray structure of **1**.

HRESIMS data (*m/z* 529.1564 [M−H]⁻, calcd. 529.1563). The 1D NMR data (Table 1) of **2** were virtually identical to those of **1**, apart from the extra methyl group instead of the alcohol group. The structure was supported by the key HMBC correlations (Fig. 2) from δ_H 3.69 (H-8) to 175.4 (C-7). The stereochemistry of **2** was determined to be the same as **1** based on the biogenetic considerations and by comparison the NMR spectra. Thus, the structure of **2** was established as chlorogenic acid methyl ester-4′-O-β-D-glucopyranoside.

Compound **9** was purified as a white amorphous powder with the molecular formula of $C_{26}H_{32}O_{13}$, deduced from the positive HRESIMS data (*m/z* 551.1770 [M−H]⁻, calcd. 551.1770). The 1D NMR data (Table 2) showed high similarity

to those of **10** with the main exception being at C-6 to C-9. Inspection of 1D and 2D NMR of **9** revealed that the compound possessed the same planar structure as that of **10** (Fig. 2). We could conclude that **9** and **10** are diastereomers with different configurations at C-7 and C-8. Compound **10** could be intended to be glehlinoside C (Yuan et al., 2002), but the configurations at C-7 and C-8 of glehlinoside C have not been identified in the literature. The relative configuration between C-7 and C-8 in **9** and **10** were determined by the well-established empirical rules in three different ways (Joon et al., 2021). First, the $\delta_{H9a-H9b}$ value of *threo*-isomers is larger than that of *erythro*-isomers. As shown in Table 2, we observed the bigger $\delta_{H9a-H9b}$ value in **9** (0.28 ppm) than that in **10** (signals of
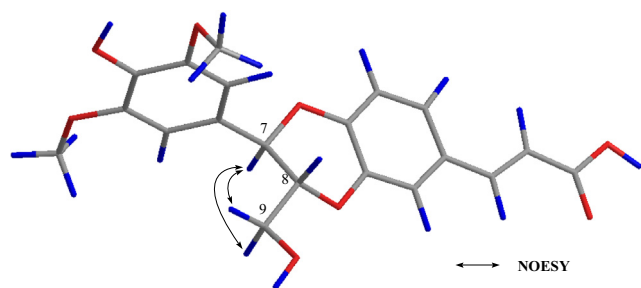
Fig. 4 Key NOESY correlations of compound **17**.

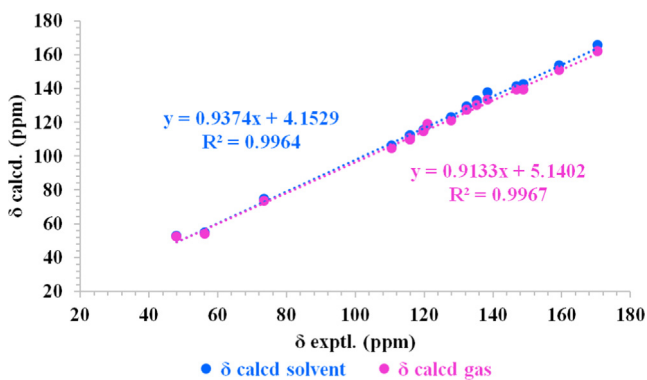**Fig. 5** Linear correlation plots of calculated and experimental ^{13}C NMR data of compound **22**.

δ_{H9a} and δ_{H9b} are overlapped). Second, $\Delta\delta_{C8-C7}$ of *threo*-isomer (12.4 ppm of **9**) was bigger than that of *erythro*-isomer (11.5 ppm of **10**). Finally, the conventional method comparing coupling constants between H-7 and H-8 was applied to confirm their relative configuration (Antonio et al., 1984). Collectively, based on these three different empirical rules the relative configuration between C-7 and C-8 were assigned as *threo* for **9** and as *erythro* for **10**. The absolute configurations of **9** and **10** were assigned by CD data analysis. The positive and negative Cotton effects at ~230–240 nm indicate 8S and 8R configuration, respectively, in 8-O-4' neolignan

derivatives (Huo et al., 2008). Observing a positive Cotton effect at 240 nm from **9** (Fig. S25) and 238 nm from **10** (Fig. S73), we assigned the absolute configuration of **9** and **10** as 8S. Collectively, the structure of **9** was elucidated as (7R,8S)-*threo*-glehlinoside C, and the structure of **10** was further elucidated as (7S,8S)-*erythro*-glehlinoside C. Compounds **11** and **12** as the aglycone of compounds **10** and **9** respectively were further elucidated as (7S,8S)-*erythro*-guaiacylglycerol-β-ferulic acid ether (**11**) and (7R,8S)-*threo*-guaiacylglycerol-β-ferulic acid ether (**12**).

Compound **13** was obtained as a white amorphous powder with a molecular formula of $C_{26}H_{30}O_{12}$ as determined by the HRESIMS (m/z 533.1664 [M−H]⁻, calcd. 533.1664). The ^{1}H NMR data of **13** (Table 2) showed a set of ABX systems at δ_H 7.14 (H-5), 7.02 (H-2), and 6.93 (H-6), and two *meta*-aromatic protons at δ_H 7.54 (H-2') and 7.20 (H-6'). Two olefinic protons at δ_H 6.83 (H-7') and 5.82 (H-8') were observed, and the Z stereochemistry was assigned based on the coupling constants between H-7' and H-8' (12.8 Hz). In addition, the presence of two methoxyl signals at δ_H 3.87 (3'-OCH₃) and δ_H 3.83 (3-OCH₃) was observed. The ^{13}C NMR data of **13** (Table 2) showed 26 carbon signals including a group of β-glucose at δ_C 102.7, 78.2, 77.8, 74.9, 71.3, 62.5, and two methoxyl signals at δ_C 56.7 (3'-OCH₃ and 3-OCH₃). The remaining 18 carbons suggested that it may be a homodimer consisting of two phenylpropyl units. The ^{1}H–^{1}H COSY correlations (Fig. 2) of **13** established the connection of C-7—C-8—C-9. The HMBC correlations (Fig. 2) from δ_H 5.63 (H-7) to 111.2 (C-2), 119.4 (C-6), and 150.6 (C-4'), and from δ_H 3.48 (H-8) to 129.4 (C-5') confirmed the presence of a pyranoid ring. Then **13** was elucidated as a benzofuran type neolignan. In addition, the HMBC correlations from δ_H 4.87 (H-1'') to 147.7 (C-4), δ_H 3.87 (3'-OCH₃) to 144.9 (C-3'), and δ_H 3.83 (3-OCH₃) to 151.0 (C-3) established the connection of the β-glucose and two methoxyl. From the $J_{H7, H8}$ (5.8 Hz) coupling constant of **13**, it was exhibited that the configurations of H-7 and H-8 were *trans*. Observing a positive Cotton effect at 238 nm from **13** (Fig. S34), the absolute configuration of 7S, 8R were assigned (Lemiére et al., 1995; Noriko et al., 1996). Therefore, compound **13** was identified as Z-(7S,8R)-aegineoside.

Compound **17** was obtained as a white amorphous powder with a molecular formula of $C_{20}H_{20}O_8$ as determined by the

Table 4 The half maximal inhibitory concentration (IC₅₀) of compounds **1-51**[a] inhibiting NO production in LPS-induced raw 264.7 cells.

| No.	IC₅₀ (μM)	No.	IC₅₀ (μM)	No.	IC₅₀ (μM)	No.	IC₅₀ (μM)
1	> 50	**14**	18.21 ± 1.93	**27**	17.52 ± 1.70	**40**	24.76 ± 1.97
2	> 50	**15**	22.57 ± 2.09	**28**	21.68 ± 2.35	**41**	> 50
3	38.35 ± 4.01	**16**	34.68 ± 3.81	**29**	42.72 ± 4.31	**42**	25.78 ± 2.41
4	18.54 ± 1.94	**17**	19.69 ± 1.91	**30**	27.56 ± 2.62	**43**	47.59 ± 4.63
5	15.10 ± 1.59	**18**	14.73 ± 1.42	**31**	> 50	**44**	> 50
6	11.97 ± 1.25	**19**	21.63 ± 1.94	**32**	10.46 ± 1.13	**45**	30.07 ± 2.99
7	19.83 ± 1.83	**20**	24.75 ± 2.46	**33**	15.31 ± 1.52	**46**	> 50
8	> 50	**21**	29.74 ± 2.92	**34**	13.03 ± 1.32	**47**	> 50
9	> 50	**22**	12.23 ± 1.20	**35**	26.33 ± 2.76	**48**	20.86 ± 2.34
10	> 50	**23**	15.75 ± 1.34	**36**	40.87 ± 4.22	**49**	26.23 ± 2.87
11	19.72 ± 1.81	**24**	12.22 ± 1.19	**37**	28.14 ± 2.67	**50**	32.36 ± 3.12
12	15.03 ± 1.51	**25**	19.45 ± 1.84	**38**	> 50	**51**	38.44 ± 3.74
13	12.33 ± 1.21	**26**	16.32 ± 1.78	**39**	25.16 ± 2.63	indomethacin	2.24 ± 0.26

[a] Data are shown as the mean ± SD, n = 3.
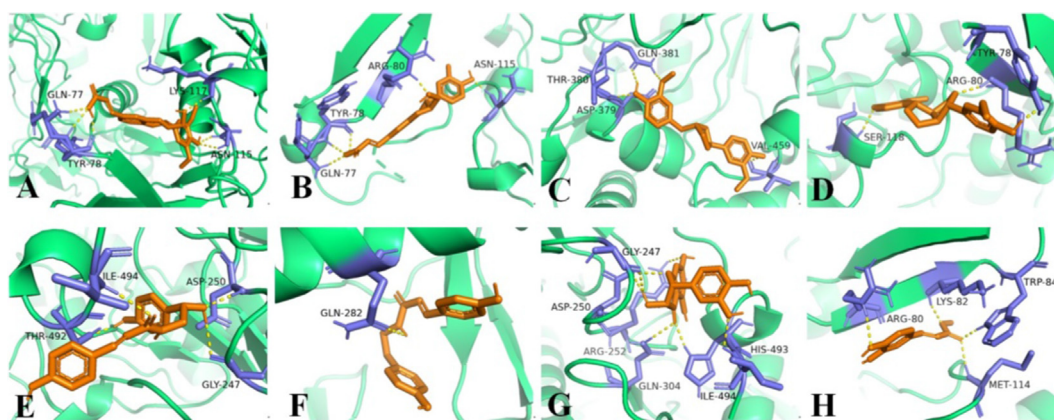
Fig. 6 Molecular docking simulations of compounds **17** (A), **18** (B), **19** (C), **20** (D), **26** (E), **27** (F), **32** (G), and **34** (H) with iNOS (3HR4). The hydrogen bonds interactions are shown by yellow dashed lines.

HRESIMS (m/z 389.1240 [M + H]$^+$, calcd. 389.1231). The ^{13}C NMR spectroscopic features of **17** (Table 3) were similar to those of the known compound (7R, 8R)-3-methoxy-8′-car boxy-7′-en-3′, 8-epoxy-7, 4′-oxyneolignan-4, 9-diol (**18**), except for one more methoxy signal at δ_C 56.9 in **17**. Moreover, the ^{1}H NMR spectrum showed that two *meta*-aromatic protons at δ_H 6.74 (H-2 and H-6) appeared in **17** (Table 3) instead of a set of ABX systems at δ_H 7.01 (H-2′), 6.91 (H-6′), and 6.84 (H-5′) in **18** (Fig. S84). Therefore, **17** was speculated to have one more methoxy group at C-5, which was further confirmed by the HMBC correlation from δ_H 3.86 (5-OCH$_3$) to δ_C 149.5 (C-5) (Fig. 2). From the NOESY correlations (Fig. 4) of H-7 (δ_H 4.94) / H-9a (δ_H 3.49) and H-7 (δ_H 4.94) / H-9b (δ_H 3.72), it was exhibited that the configurations of H-7 and H-8 were *trans*. The configurations of C-7 and C-8 of compound **17** were further determined to be 7R and 8R consistent with that of compound **18** based on NMR / OR data comparison and biosynthesis (Zhou et al., 2015). Accordingly, compound **17** was characterized as (7R,8R)-3,5-dimethoxy-8′-carboxy-7′-en-3′,8-epoxy-7,4′-oxyneolignan-4,9-diol.

Compound **22** was obtained as a white amorphous powder. It showed an [M−H]$^-$ ion at m/z 328.1183 (calcd. 328.1190) in the HRESIMS spectrum, giving a molecular formula of C$_{18}$H$_{19}$NO$_5$. The HMBC correlation from δ_H 3.84 (3′-OCH$_3$)

Fig. 7 Venn diagram containing the inflammation-related targets (A) and compounds-related targets (B).

to δ_C 148.9 (C-3′) (Fig. 2), and comparison with the known compound *N-cis-p*-coumaroyloctopamine (**24**) confirmed that compound **22** had an extra methoxy group connected to C-3′.

The configurations of C-7′ of compound **22** were determined by an NMR calculation with DP4$^+$ analysis. The shielding tensors of two possible isomers 7′R and 7′S were predicted using the GIAO method at the mPW1PW91/6-31G*// B3LYP/6-31G* (in the gas phase) and mPW1PW91/6-31G**//B3LYP/6-31G* (in methanol) levels. The results showed that 7′R was the most likely candidate structure (Fig. 5, Figs. S157-158). Thus, the configurations of C-7′ of compound **22** were determined to be 7′R. The structure of compound **22** was determined as 3-(4-hydroxy)-*N*-[2-(3-meth oxyphenyl-4-hydroxyphenyl)-2- hydroxy]acrylamide.

Compound **40**, amorphous powder, possesses a molecular formula of C$_{16}$H$_{19}$NO$_7$ based on its HRESIMS m/z 355.1493 [M + NH$_4$]$^+$ (calcd. 355.1500). According to the ^{1}H and ^{13}C NMR spectra, the aglycone of compound **40** is the same as that of hydranitriloside B2 (**41**). There is an extra acetyl group connected to the hydroxy group of C-6′ in **40**, which was determined by the HMBC correlations from δ_H 4.23 (H-6′) to δ_C 172.7 (C-1″) (Fig. 2). Compound **40** was therefore identified as *p*-hydroxyphenylacetonitrile-O-(6′-O-acetyl)-*β*-D-glucopyranoside.

3.2. Anti-inflammatory effects

Nitric oxide (NO) is known to be a potent pro-inflammatory mediator and possesses a dual regulatory function in the inflammatory reaction (Lee et al., 2017a; Lee et al., 2018). NO plays anti-inflammatory roles under normal physiological conditions, however, excessive production of NO has been found associated with various inflammatory disorders (Hu et al., 2020; Tang et al., 2020). Considering the traditional efficacy of *Solanum xanthocarpum* and the goal to obtain NO inhibitors to treat the inflammatory disorder, the inhibitory effects of compounds **1–51** isolated from *Solanum xanthocarpum* fruits on NO production in LPS-induced RAW 264.7 macrophages were evaluated. Indomethacin, a non-steroidal anti-inflammatory drug, was selected as a standard control. As showed in Table 4, compounds **3–7**, **11–30**, **32–37**, **39**, **40**, **42**, **43**, **45**, and **48–51** exerted the significant inhibition of
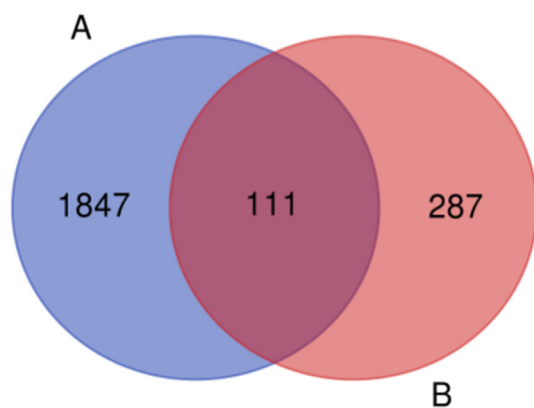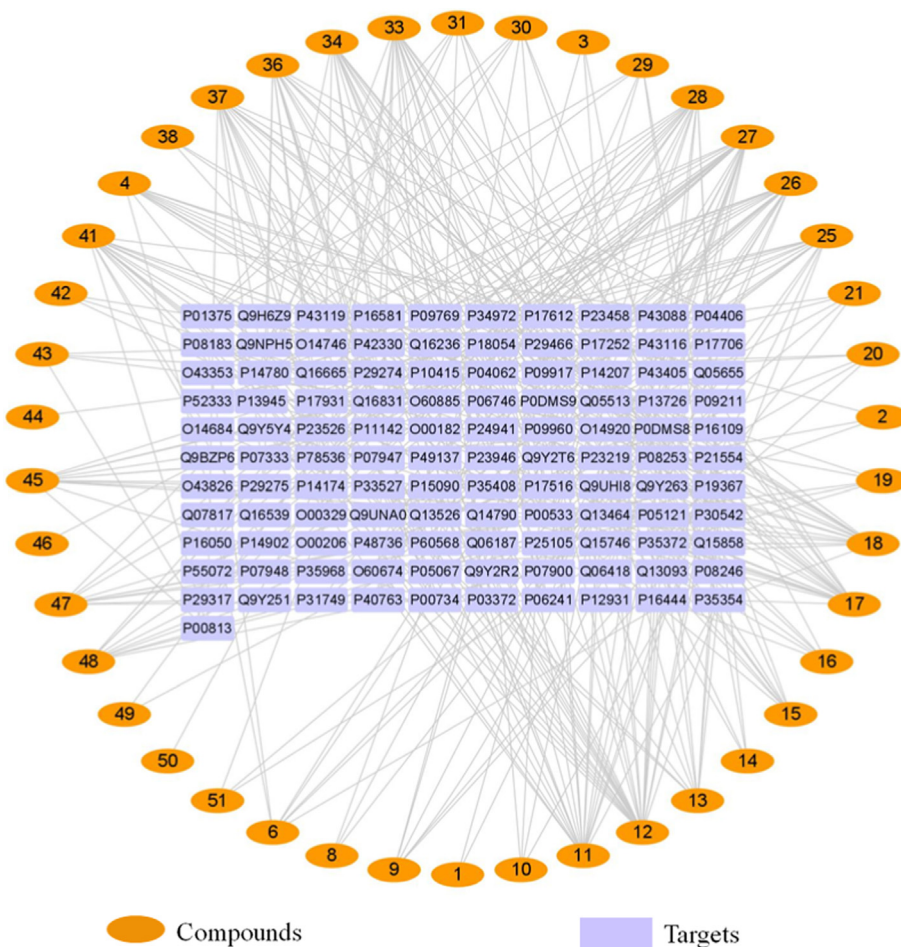
Fig. 8   Compound-target network diagram.

LPS-induced NO production in RAW 264.7 cells, with IC_{50} values ranging from 10.46 to 47.59 μM. New compounds **9**, **13**, **17**, **22**, and **40** showed outstanding activity, especially **13** (IC_{50} 12.33 μM) and **22** (IC_{50} 12.23 μM).

3.3. Molecular docking studies

The release of NO is mainly regulated by eNOS, nNOS, and iNOS, of which iNOS is vital to the release of NO and regulates the amount of NO in inflammatory processes (Lee et al., 2017b). To investigate the possible mechanism inhibiting NO production, molecular docking studies were conducted to investigate the interactions between the bioactive compounds and iNOS proteins. The bioactive compounds **3–7**, **11–30**, **32–37**, **39**, **40**, **42**, **43**, **45**, and **48–51** were selected for molecular docking studies, and the results revealed that almost all compounds had good affinities [Log (FBE) < -5 kJ/mol] with iNOS proteins (Table S2). Especially, compounds **17–20**, **26–27**, **32**, and **34** showed strong affinities with iNOS proteins, with affinities comparable to indomethacin (Table S2 and Fig. 6).

3.4. Bioinformatic analysis

A total of 1958 inflammation-related targets were identified from UniProt. 398 possible targets for the ''Homo sapiens''

species of 42 compounds were attained by using SwissTargetPrediction to screen and remove repetition. Fig. 7 shows the Venn diagram of the compound and inflammation targets, such that the common part of the two was regarded as to include potential anti-inflammatory targets. There were 111 overlapping targets between the compound targets and inflammation-related targets. The correlations between the compound targets and overlapping targets were constructed and visualized by Cytoscape 3.7.2 software (Fig. 8 and Table S1). The results show that the 9 targets with a higher degree value among the anti-inflammatory targets are adenosine receptor A2a (P29274, degree = 18), adenosine receptor A1 (P30542, degree = 16), 72 kDa type IV collagenase (P08253, degree = 15), adenosine receptor A3 (P0DMS8, degree = 14), matrix metalloproteinase-9 (P14780, degree = 13), prostaglandin G/H synthase 2 (P35354, degree = 12), prostaglandin G/H synthase 1 (P23219, degree = 11), cannabinoid receptor 2 (P34972, degree = 10), and epidermal growth factor receptor (P00533, degree = 10), which play a major role in the network.

4. Conclusions

The present work first systemically isolated and identified the phenolic compounds from the fruits of *Solanum xanthocarpum*. In conclusion, 51 phenolic compounds including seven new compounds **1**, **2**, **9**, **13**, **17**, **22**, and **40** and 40 known compounds **3–8**, **10–12**, **14–16**, **18–21**,

23–25, 28–32, 35–39, 41–51 firstly isolated from *Solanum xantho-carpum*. Biological studies disclosed that most isolates exhibited significant anti-inflammatory effects by inhibiting LPS-induced NO production, especially (+)-taxifolin (**32**), chlorogenic acid and its derivatives (**4–7**), caffeic acid and its derivatives (**33–34**), phenylacrylamides (**22–28**), and some lignans (**11–14, 17, 18**). Molecular docking revealed that compounds **17–20, 26–27, 32**, and **34** showed strong affinities with iNOS proteins by targeting the residues of the active cavities of iNOS, with affinities comparable to the positive control indomethacin. In addition, bioinformatic analysis disclosed that phenolic compounds may act on many other inflammation-related targets, and adenosine receptor A2a, adenosine receptor A1, 72 kDa type IV collagenase, adenosine receptor A3, matrix metalloproteinase-9, prostaglandin G/H synthase 2, prostaglandin G/H synthase 1, cannabinoid receptor 2, and epidermal growth factor receptor may be the key anti-inflammatory targets. These findings supported the phenolic compounds as the important anti-inflammatory ingredients of *Solanum xanthocarpum* fruits, which provide the scientific basis for the sustainable development and usage of the resources of *Solanum xanthocarpum*.

Declaration of Competing Interest

The authors declare that they have no known competing financial interests or personal relationships that could have appeared to influence the work reported in this paper.

Acknowledgments

Appendix A. Supplementary material

Supplementary data to this article can be found online at https://doi.org/10.1016/j.arabjc.2022.103877.

References

Abdallah, H.M., Al-Abd, A.M., Asaad, G.F., Abdel-Naim, A.B., El-halawany, A.M., 2014. Isolation of antiosteoporotic compounds from seeds of *Sophora japonica*. PLoS ONE 9 (6), e98559. https://doi.org/10.1371/journal.pone.0098559.

Al-Taweel, A.M., Perveen, S., El-Shafae, A.M., Fawzy, G.A., Malik, A., Afza, N., Iqbal, L., Latif, M., 2012. Bioactive phenolic amides from *Celtis africana*. Molecules 17 (3), 2675–2682. https://doi.org/10.3390/molecules17032675.

Ambriz-Pérez, D.L., Leyva-López, N., Gutierrez-Grijalva, E.P., Heredia, J.B., Basilio, J., Yildiz, F., 2016. Phenolic compounds: Natural alternative in inflammation treatment. A Review, Cogent Food Agr. 2 (1), 1131412. https://doi.org/10.1080/23311932.2015.1131412.

Antonio, C.H.B., Susana, Z., Héctor, B., Manuel, G.S., Edmundo, A.R., 1984. ^{13}C NMR spectral and conformational analysis of 8-O-4′ neolignans. Phytochemistry 23 (9), 2025–2028. https://doi.org/10.1016/S0031-9422(00)84963-8.

Barakat, A.Z., Hamed, A.R., Bassuiny, R.I., Abdel-Aty, A.M., Mohamed, S.A., 2020. Date palm and saw palmetto seeds functional properties: antioxidant, anti-inflammatory and antimicrobial activities. J. Food Meas. Charact. 14, 1064–1072. https://doi.org/10.1007/s11694-019-00356-5.

Chen, Y.H., Chang, F.R., Lin, Y.J., Wang, L., Chen, J.F., Wu, Y.C., Wu, M.J., 2008. Identification of phenolic antioxidants from Sword Brake fern (*Pteris ensiformis* Burm.). Food Chem. 105 (1), 48–56. https://doi.org/10.1016/j.foodchem.2007.03.055.

Crupi, P., Bleve, G., Tufariello, M., Corbo, F., Clodoveo, M.L., Tarricone, L., 2018. Comprehensive identification and quantification of chlorogenic acids in sweet cherry by tandem mass spectrometry techniques. J. Food Compos. Anal. 73, 103–111. https://doi.org/10.1016/j.jfca.2018.06.013.

Ding, Y., Liang, C., Choi, E.M., Ra, J.C., Kim, Y.H., 2011. Chemical constituents from *Artemisia iwayomogi* increase the function of osteoblastic MC3T3-E1 cells. Nat. Prod. Sci. 15 (4), 92–197.

Fu, J., Wang, H., Dong, C.X., Xi, C., Xie, J., Lai, S., Chen, R., Kang, J., 2021. Water-soluble alkaloids isolated from *Portulaca oleracea* L. Bioorg. Chem. 113, 105023. https://doi.org/10.1016/j.bioorg.2021.105023.

Grimblat, N., Zanardi, M.M., Sarotti, A.M., 2015. Beyond DP4: an Improved Probability for the Stereochemical Assignment of Isomeric Compounds using Quantum Chemical Calculations of NMR Shifts. J. Org. Chem. 80, 12526–12534. https://doi.org/10.1021/acs.joc.5b02396.

He, T., Zhao, Y.C., Li, P.Y., Weng, Z.Y., Chang, Y.L., Chen, X.Y., Bai, S.J., Liu, Z.Z., She, G.M., 2017. Chemical constituents from anti-inflammatory and analgesic active fraction of *Gaultheria leucocarpa* var. yunnanensis. Chinese Trad. Herbal Drugs 48 (17), 3469–3474. https://doi.org/10.7501/j.issn.0253-2670.2017.17.003.

Hu, Y.S., Han, X., Yu, P.J., Jiao, M.M., Liu, X.H., Shi, J.B., 2020. Novel paeonol derivatives: Design, synthesis and anti-inflammatory activity in vitro and in vivo. Bioorg. Chem. 98, 103735. https://doi.org/10.1016/j.bioorg.2020.103735.

Huo, C.H., Liang, H., Zhao, Y.Y., Wang, B., Zhang, Q.Y., 2008. Neolignan glycosides from *Symplocos caudata*. Phytochemistry 69 (3), 788–795. https://doi.org/10.1016/j.phytochem.2007.08.022.

Iclal, S., Mehtap, V., Ihsan, Ç., Ali, D., 2003. Neolignan, Flavonoid, Phenylethanoid and Iriloid Glycosides from *Phlomis integrifolia*. Turk. J. Chem. 27 (6), 739–747.

Jin, M., Zhang, C.H., Zheng, T., Yao, D., Shen, L., Luo, J., Jiang, Z., Ma, J., Jin, X.J., Cui, J.M., Lee, J.J., Li, G., 2014. A new phenyl glycoside from the aerial parts of *Equisetum hyemale*. Nat. Prod. Res. 28 (21), 1813–1818. https://doi.org/10.1080/14786419.2014.947491.

Joon, M.C., Tae, H.L., Lalita, S., Young, J.H., Hye, R.K., Sun, Y.K., Sang, U.C., Chung, S.K., 2021. Isolation and structural characterization of four diastereomeric lignan glycosides from *Abies holophylla* and their neuroprotective activity. Tetrahedron 77, 131735. https://doi.org/10.1016/j.tet.2020.131735.

Kar, D.M., Maharana, L., Pattnaik, S., Dash, G.K., 2006. Studies on hypoglycaemic activity of *Solanum xanthocarpum* Schrad. & Wendl. fruit extract in rats. J. Ethnopharmacol. 108 (2), 251–256. https://doi.org/10.1016/j.jep.2006.05.016.

Kuang, H.X., Tang, Z.Q., Wang, X.G., Yang, B.Y., Wang, Z.B., Wang, Q.H., 2018. Chemical constituents from *Sambucus williamsii* Hance fruits and hepatoprotective effects in mouse hepatocytes. Nat. Prod. Res. 32 (17), 2008–2016. https://doi.org/10.1080/14786419.2017.1361948.

Lee, E.J., Kim, J.S., Kim, H.P., Lee, J.H., Kang, S.S., 2010. Phenolic constituents from the flower buds of *Lonicera japonica* and their 5-lipoxygenase inhibitory activities. Food Chem. 120 (1), 134–139. https://doi.org/10.1016/j.foodchem.2009.09.088.

Lee, S., Lee, D., Lee, J.C., Kang, K.S., Ryoo, R., Park, H.J., Kim, K.H., 2018. Bioactivity-guided Isolation of Anti-inflammatory Constituents of the Rare Mushroom *Calvatia nipponica* in LPS-stimulated RAW264.7 Macrophages. Chem. Biodivers. 15 (9), e1800203. https://doi.org/10.1002/cbdv.201800203.

Lee, S., Lee, D., Lee, S.O., Ryu, J.Y., Choi, S.Z., Kang, K.S., Kim, K.H., 2017a. Anti-inflammatory activity of the sclerotia of edible fungus, *Poria cocos* Wolf and their active lanostane triterpenoids. J. Funct. Foods 32, 27–36. https://doi.org/10.1016/j.jff.2017.02.012.

Lee, S.R., Lee, S., Moon, E., Park, H.J., 2017b. Bioactivity-guided isolation of anti-inflammatory triterpenoids from the sclerotia of *Poria cocos* using LPS-stimulated Raw264.7 cells. Bioorg. Chem. 70, 94–99. https://doi.org/10.1016/j.bioorg.2016.11.012.

Lemiére, G.L.F., Gao, M., de Groot, A.H.J., Dommisse, R.A., Lepoivre, J.A., Pieters, L.A., Buß, V., 1995. 3′,4-Di-O-methyl-cedrusin: synthesis, resolution and absolute configuration. J. Chem. Soc., Perkin Trans. 1 (13), 1775–1779. https://doi.org/10.1039/P19950001775.

Li, L.H., Ren, F.Z., Chen, S.H., Gao, Y.Q., 2009. New homoisoflavanones from Polygonatum odoratum (Mill.) Druce, Acta. Pharm. Sin. B 44 (7), 764–767.

Li, R.X., Cheng, J.T., Jiao, M.J., Zhang, J., Chen, S., Guo, C., Liu, A., 2017. Chemical constituents from leaves of Uncaria rhynchophylla. Chinese Trad. Herbal Drugs 48 (8), 1499–1505. https://doi.org/10.7501/j.issn.0253-2670.2017.08.003.

Li, S., Hu, L.H., Lou, F.C., 2004. Study on the chemical constituents of Saussurea lappa. Chin. J. Nat. Med. 2 (1), 62–64.

Liang, D., Hao, Z.Y., Liu, Y.F., Luo, H., Wang, Y., Zhang, C.L., Zhang, Q.J., Chen, R.Y., Yu, D.Q., 2013. Bioactive carboxylic acids from Lysimachia clethroides. J. Asian Nat. Prod. Res. 15 (1), 59–66. https://doi.org/10.1080/10286020.2012.745855.

Liang, Y.H., Ye, M., Zhang, L.Z., Li, H.F., Han, J., Wang, B.R., Guo, D.A., 2010. Two new phenolic acids from Drynariae rhizoma. Yao Xue Xue Bao 45 (7), 874–878.

Liu, X., Yin, C.L., Cao, Y., Zhou, J.G., Wu, T., Cheng, Z.H., 2018. Chemical constituents from Gueldenstaedtia verna and their anti-inflammatory activity. Nat. Prod. Res. 32 (10), 1145–1149. https://doi.org/10.1080/14786419.2017.1320795.

Lou, H., Yuan, H., Yamazaki, Y., Sasaki, T., Oka, S., 2001. Alkaloids and flavonoids from peanut skins. Planta Med. 67 (4), 345–349. https://doi.org/10.1055/s-2001-14319.

Ma, C.H., Whitaker, B.D., Kennelly, E.J., 2010. New 5-O-Caffeoylquinic Acid Derivatives in Fruit of the Wild Eggplant Relative Solanum viarum. J. Agr. Food. Chem. 58 (20), 11036–11042. https://doi.org/10.1038/sj.ki.5002362.

More, S.K., Lande, A.A., Jagdale, P.G., Adkar, P.P., Ambavade, S.D., 2013. Evaluation of anti-inflammatory activity of Solanum xanthocarpum Schrad and Wendl (Kaṇṭakārī) extract in laboratory animals. Anc. Sci. Life 32 (4), 222–226. https://doi.org/10.4103/0257-7941.131976.

Nakamura, S., Zhang, Y., Wang, T., Matsuda, H., Yoshikawa, M., 2008. New phenolic glycosides from the leaves of Salacia chinensis. Heterocycles 75 (6), 1435–1446. https://doi.org/10.3987/COM-08-11338.

Noriko, M., Hiromi, S., Yasunori, Y., Masao, K., 1996. Isolation and absolute structures of the neolignan glycosides with the enantiometric aglycones from the leaves of Viburnum awabuki K. KOCH. Chem. Pharm. Bull. 44 (5), 1122–1123. https://doi.org/10.1248/cpb.44.1122.

Ono, M., Shiono, Y., Yanai, Y., Fujiwara, Y., Ikeda, T., Nohara, T., 2008. A new steroidal glycoside and a new phenyl glycoside from a ripe cherry tomato. Chem. Pharm. Bull. 56 (10), 1499–1501. https://doi.org/10.1248/cpb.56.1499.

Parmar, K.M., Itankar, P.R., Joshi, A., Prasad, S.K., 2017. Anti-psoriatic potential of Solanum xanthocarpum stem in Imiquimod-induced psoriatic mice model. J. Ethnopharmacol. 198, 158–166. https://doi.org/10.1016/j.jep.2016.12.046.

Periyannan, V., Annamalai, V., Perumal, I., Dhananjayan, I., 2016. Evaluation of antioxidant and stabilizing lipid peroxidation nature of Solanum xanthocarpum leaves in experimentally diethylnitrosamine induced hepatocellular carcinogenesis. Biomed. Pharmacother. 84 (1), 430–437. https://doi.org/10.1016/j.biopha.2016.09.060.

Ralf, L., Joachim, S., Heinz, K., 1993. p-Hydroxyphenyl-O-β-D-primeveroside, a Novel Glycoside Formed from Hydroquinone by Cell Suspension Cultures of Rauwolfia serpentina. J. Nat. Prod. 56 (8), 1421–1422. https://doi.org/10.1021/np50098a029.

Saimaru, H., Orihara, Y., 2010. Biosynthesis of acteoside in cultured cells of Olea europaea. J. Nat. Med.-Tokyo 64 (2), 139–145. https://doi.org/10.1007/s11418-009-0383-z.

Sasaki, K., Takahashi, T., 2002. A flavonoid from Brassica rapa flower as the UV-absorbing nectar guide. Phytochemistry 61 (3), 339–343. https://doi.org/10.1016/S0031-9422(02)00237-6.

Shen, G.H., Kiem, P.V., Cai, X.F., Li, G., Dat, N.T., Choi, Y., Lee, Y.M., Park, Y.K., Kim, Y.H., 2005. Solanoflavone, a new biflavonol glycoside from Solanum melongena: Seeking for anti-inflammatory components. Arch. Pharm. Res. 28 (6), 657–659. https://doi.org/10.1007/BF02969354.

Shen, Y.X., Teng, H.L., Yang, G.Z., Mei, Z.N., Chen, X.L., 2010. A new chromone derivative from Berchemia lineata. Yao Xue Xue Bao 45 (9), 1139–1143.

Shivnath, N., Siddiqui, S., Rawat, V., Khan, M.S., Arshad, M., 2021. Solanum xanthocarpum fruit extract promotes chondrocyte proliferation in vitro and protects cartilage damage in collagenase induced osteoarthritic rats. J. Ethnopharmacol. 274, 114028. https://doi.org/10.1016/j.jep.2021.114028.

Takeda, Y., Ooiso, Y., Masuda, T., Honda, G., Otsuka, H., Sezik, E., Yesilada, E., 1998. Iridoid and eugenol glycosides from Nepeta cadmea. Phytochemistry 49 (3), 787–791. https://doi.org/10.1016/S0031-9422(98)00125-3.

Tang, Y.L., Zheng, X., Qi, Y., Pu, X.J., Liu, B., Zhang, X., Li, X.S., Xiao, W.L., Wan, C.P., Mao, Z.W., 2020. Synthesis and anti-inflammatory evaluation of new chalcone derivatives bearing bispiperazine linker as IL-1β inhibitors. Bioorg. Chem. 98, 103748. https://doi.org/10.1016/j.bioorg.2020.103748.

Uyang, M.A., Chen, P.Q., Wang, S.B., 2007. Water-soluble phenylpropanoid constituents from aerial roots of Ficus microcarpa. Nat. Prod. Res. 21 (9), 769–774. https://doi.org/10.1080/14786410500462611.

Wang, L.Y., Qu, Y.H., Li, Y.C., Wu, Y.Z., Li, R., Guo, Q.L., Wang, S.J., Wang, Y.N., Yang, Y.C., Lin, S., 2017. Water soluble constituents from the twigs of Litsea cubeba. China J. Chinese Materia Medica 42 (14), 2704–2713 https://doi.org/10.19540/j.cnki.cjcmm.2017.0119.

Wang, Z.B., Gao, H.Y., Yang, C.J., Sun, Z., Wu, L.J., 2011. Novel Cyanoglucosides from the Leaves of Hydrangea macrophylla. Helv. Chim. Acta 94 (5), 847–852. https://doi.org/10.1002/hlca.201000314.

Xiao, Y.Y., Gou, P., Xie, H.H., 2017. Phenylpropanoids from Lentopodium lenotopodioides. J. Trop. Subtropical Botany 25 (2), 195–201 https://doi.org/10.11926/jtsb.3649.

Yang, B.Y., Luo, Y.M., Liu, Y., Yin, X., Zhou, Y.Y., Kuang, H.X., 2018. New lignans from the roots of Datura metel L. Phytochem. Lett. 28, 8–12. https://doi.org/10.1016/j.phytol.2018.08.002.

Yang, Y.C., Wu, X.X., Meng, Y.L., Qin, Y., Xia, C.F., Hu, Q.F., Li, Y.K., 2015. Chemical constituents from Lindera caudata (Nees) Hook. f. Chinese Trad. Patent Med. 37 (11), 2455–2458. https://doi.org/10.16438/j.0513-4870.2004.04.008.

Yin, X., Liu, Y., Pan, J., Ye, H.L., Sun, Y., Zhao, D.Y., Kuang, H.X., Yang, B.Y., 2019. Melongenaterpenes A-L, Vetispirane-Type Sesquiterpenoids from the Roots of Solanum melongena. J. Nat. Prod. 82 (12), 3242–3248. https://doi.org/10.1021/acs.jnatprod.9b00206.

Yin, X., Zhang, Q., Zhang, H.X.G., Wuken, S.N., Li, J.J., Jiao, S.G., Yang, F.Q., Tu, P.F., Chai, X.Y., 2018. Chemical constituents from a Tibetan herbal medicine Corydalis hendersonii. China J. Chinese Materia Medica 43 (9), 1758–1763 https://doi.org/10.19540/j.cnki.cjcmm.20180115.014.

Yuan, Z., Tezuka, Y., Fan, W.Z., Kadota, S., Li, X., 2002. Constituents of the Underground Parts of Glehnia littoralis. Chem. Pharm. Bull. 50 (1), 73–77. https://doi.org/10.1248/cpb.50.73.

Zhang, Y., Chen, Q., Liu, L.L., Deng, S., Qu, L., Wang, T., 2013a. Isolation and identification of chemical constituents from Althaea rosea (Linn.) Cavan. (I). J. Shenyang Pharm. Univ. 30 (5), 335–341 https://doi.org/10.14066/j.cnki.cn21-1349/r.2013.05.004.

Zhang, M., Liu, W.X., Zheng, M.F., Xu, Q.L., Wan, F.H., Wang, J., Lei, T., Zhou, Z.Y., Tan, J.W., 2013b. Bioactive quinic acid

derivatives from *Ageratina adenophora*. Molecules 18 (11), 14096–14104. https://doi.org/10.3390/molecules181114096.

Zhang, Y., Liu, J.Z., Wang, M.Y., Sun, C.J., Li, X.B., 2020. Five new compounds from *Hosta plantaginea* flowers and their anti-inflammatory activities. Bioorg. Chem. 95, 103494. https://doi.org/10.1016/j.bioorg.2019.103494.

Zhao, D.B., Zhang, W., Li, M.J., Liu, X.H., 2006. Studies on chemical constituents of *Acroptilon repens*. Zhongguo Zhong Yao Za Zhi 31 (22), 1869–1872.

Zhao, D.Y., Liu, Y., Yin, X., Li, X.M., Pan, J., Guan, W., Yang, B.Y., Kuang, H.X., 2021. Two new alkaloids from the sepals of Solanum melongena L. Nat. Prod. Res. 35 (21), 3569–3577. https://doi.org/10.1080/14786419.2020.1713126.

Zhao, X.H., Chen, D.H., Si, J.Y., Pan, R.L., Shen, L.G., 2002. Studies on the phenolic acid constituents from Chinese medicine sheng-ma, rhizome of *Cimicifuga foetida* L. Yao Xue Xue Bao 37 (7), 535–538.

Zhou, D.Z., Yi, Y.H., Mao, S.L., Lu, T.S., Tang, H.F., Zou, Z.R., Zhang, S.Y., 2004. The lignins from *Torreya grandis* cv. Merrilli. Acta. Pharm. Sin. B 39 (4), 269–271 https://doi.org/10.16438/j.0513-4870.2004.04.008.

Zhou, J.T., Li, C.Y., Wang, C.H., Wang, Y.F., Wang, X.D., Wang, H.T., Zhu, Y., Jiang, M.M., Gao, X.M., 2015. Phenolic Compounds from the Roots of *Rhodiola crenulata* and Their Antioxidant and Inducing IFN-γ Production Activities. Molecules 20 (8), 13725–13739. https://doi.org/10.3390/molecules200813725.

Zhu, X.D., Dong, X.J., Wang, W.F., Ju, P., Luo, S.D., 2005. Phenolic compounds from *Viburnum cylindricum*. Helv. Chim. Acta 88 (2), 339–342. https://doi.org/10.1002/hlca.200590017.